RSC Advances

PAPER

View Article Online
View Journal | View Issue

Cite this: *RSC Adv.*, 2022, **12**, 31792

Highly effective removal of Hg(II) solution using corn bract@MoS_2 as a new biomass adsorbent†

Xiaoxu Xu,‡[a] Qihui Guo,‡[b] Chengyue Yang,[b] Zhuang Hu,[b] Qifan Chen*[a] and Jianshe Hu *[b]

Received 7th September 2022
Accepted 2nd November 2022

DOI: 10.1039/d2ra05638k

rsc.li/rsc-advances

As known, mercury contamination is one of the current environmental issues due to the high toxicity of mercury. Corn bract (CB) is an agricultural by-product, and its final treatment is generally incineration that causes air pollution. In this study, a new type of high-efficiency biomass adsorbent (CB@MoS_2) for adsorption of Hg(II) was obtained, and its morphology and structure were characterized with FT-IR, XRD, SEM and TEM. The results showed that when the pH value, Hg(II) ion concentration and adsorption time were 4, 100 mg L^{-1} and 120 min, the adsorption capacity and removal rate could reach 332.50 mg g^{-1} and 99.75%. In addition, CB@MoS_2 had a good selectivity for Hg(II) ions. The adsorption behavior followed pseudo-second-order kinetics, indicating that the adsorption of Hg(II) ions by CB@MoS_2 was a chemical adsorption. After five adsorption–desorption experiments, it still possessed good adsorption performance and effective regeneration. In short, CB@MoS_2 has high efficiency and good reusability, and will become a candidate material for the treatment of mercury-containing industrial wastewater.

1. Introduction

Due to rapid industrialization and urbanization, pollution of water by heavy metals is still an issue of increasing concern.[1] Heavy metal ions (such as Hg(II)) have high toxicity, bio-accumulation and non-degradability, and their continuous emission is very harmful to the food chain and human health.[2,3] Therefore, it is necessary for us to remove heavy metals from aqueous solutions. The Hg(II) ion removal methods include adsorption, biological treatment, chemical precipitation, ion exchange, extraction and other methods.[4,5] In the process of heavy metal wastewater treatment, the precipitation method may cause secondary pollution, while the biological method and the ion exchange method are costly and poor in recycling.[6,7] In contrast, the adsorption method is widely used in the removal of heavy metal ions due to its low cost, environmental friendliness, easy operation, high efficiency, good reusability and selectivity.[8] There are usually two kinds of adsorbents for removing Hg(II): natural materials and synthetic polymers. Compared with other commercial adsorbents, the practical application of synthetic polymers with small specific surface area in removing mercury ions is limited.[9] Natural adsorbents include microbial adsorbents, inorganic mineral materials and biomass adsorbents. The adsorption capacity of inorganic mineral materials needs to be increased by chemical or physical modification. When the microbial adsorbent removes higher concentrations of mercury from wastewater, the adsorption effect is limited due to the long microbial culture cycle. Biomass adsorbents have excellent adsorption capacity for heavy metal ions existing in industrial wastewater, and are also good at renewable environmental protection.[10]

Corn bract (CB) is usually burned as an agricultural by-product, and its combustion is considered an important source of carbon in the air.[11] The large amount of carbon black produced by burning CB would make the air pollution problem more and more serious. CB contains 54–58% lignocellulose with rich hydroxyl. In addition, hydrophilicity and biodegradability were the significant merits of CB, so there are many advantages when using this material in the field of adsorption.[12] For example, CB functionalized with polyethyleneimine was used to remove hexavalent chromium in the water through the concept of "using waste to treat waste".[13]

MoS_2 is a two-dimensional nanomaterial with a lamellar structure similar to the carbon material graphene. It has a large specific surface area, acid resistance, alkali resistance, high temperature resistance, and stable chemical properties.[14,15]

In recent years, there are many metal sulfides that can be used as adsorption materials for mercury ions.[16,17] Although they have good adsorption capacity, their regeneration capacity is not ideal. Moreover, metal organic framework and other emerging porous materials with good adsorption capacity, their high cost need to be resolved.[18,19] Although MoS_2 has a good adsorption capacity for heavy metal ions,[20] its price is expensive.

[a]*College of Chemical Engineering and Machinery, Eastern Liaoning University, Dandong, 118001, P. R. China. E-mail: qifan_C405@163.com*

[b]*Center for Molecular Science and Engineering, College of Science, Northeastern University, Shenyang, 110819, P. R. China. E-mail: hujs@mail.neu.edu.cn*

† Electronic supplementary information (ESI) available. See DOI: https://doi.org/10.1039/d2ra05638k

‡ These authors contributed equally to this work.

Considering the price and adsorption effect from the practical application, we choose CB@MoS_2 composite material to investigate its adsorption behavior.

Herein, a new biomass adsorbent (CB@MoS_2) was constructed by introducing the MoS_2 onto CB though a hydrothermal method, and it was used for the adsorption of Hg(II) ions. The adsorption performance of CB@MoS_2 was inspected by exploring the effect on Hg(II) ion removal by changing the pH, adsorbent dosage, temperature, adsorption time, initial concentration and coexisting ions and other factors, then, adsorption isotherm and kinetics were applied to describe the adsorption process, finally, the mechanism of CB@MoS_2 for Hg(II) was systematically explored.

2. Experimental section

2.1. Materials and instruments

Materials and instruments see ESI (Text S1).†

2.2. Preparation of CB@MoS_2 composite material

The preparation of CB@MoS_2 composite material was shown in Fig. 1. The CB was added in an oven to remove a large amount of water, then cut and ground it into powder, and the MoS_2 was loaded on CB by hydrothermal method. First of all, 0.35 g $(NH_4)_6Mo_7O_{24}\cdot 4H_2O$ and 0.76 g CH_4N_2S were put into 15 mL of deionized water, subsequent ultrasonic treatment for 30 min to form a uniform solution. Next, 2.4 g processed CB powder was added to the above solution and magnetic stirring for 30 min to make full contact and then dispersed by ultrasonic treatment for 30 min, then the mixture was put into a stainless steel autoclave with polytetrafluoroethylene incubate at 200 °C for 8 h. Finally, the resulting black product was centrifuged multiple times, then washed with ethanol and water multiple times, and finally dried in vacuum at 60 °C for 12 h to obtain a CB@MoS_2 (the composition ratio of CB : MoS_2 was 8 : 1) composite material. To study the effect of CB content, the different amounts of CB were added the same solution as above, respectively. According to the results of cost and adsorption effect, the above ratio was selected as the best ratio, and a series of investigations on the adsorption effect of mercury ions were carried out.

2.3. Adsorption and desorption study

The adsorption performance of the prepared CB@MoS_2 was studied as follows. Firstly, to discuss the influence of pH value, 15 mg CB@MoS_2 was added to 50 mL of 100 mg L^{-1} series of solutions for adsorption experiments, and the pH of solution was adjusted from 1 to 8 with HNO_3 (0.8 mol L^{-1}) and NaOH (0.1 mol L^{-1}). Because the dosage of adsorbent has a certain effect on the adsorption of Hg(II) ions, the 5–30 mg of adsorbent was added into Hg(II) ion solution (50 mL, 100 mg L^{-1}) at pH 4. Taking the influence of the initial concentration of Hg(II) ions into account, 15 mg CB@MoS_2 was added in Hg(II) ion solution (50 mL) with a concentration of 100–500 mg L^{-1} and a pH of 4. CB@MoS_2 (15 mg) and Hg(II) ion solution (pH = 4, V = 50 mL, C = 100 mg L^{-1}) contact time (1–120 min) to evaluate the effect of adsorption time. In the above experiments, the concentration of Hg(II) ions after the adsorption process was measured by mercury vapour analyzer (CG-1C) with the method of direct reading. The adsorption capacity (Q_t) and removal rate (R) of CB@MoS_2 were measured by eqn (1) and (2).

$$Q_t = \frac{(C_0 - C_t) \times V}{m} \quad (1)$$

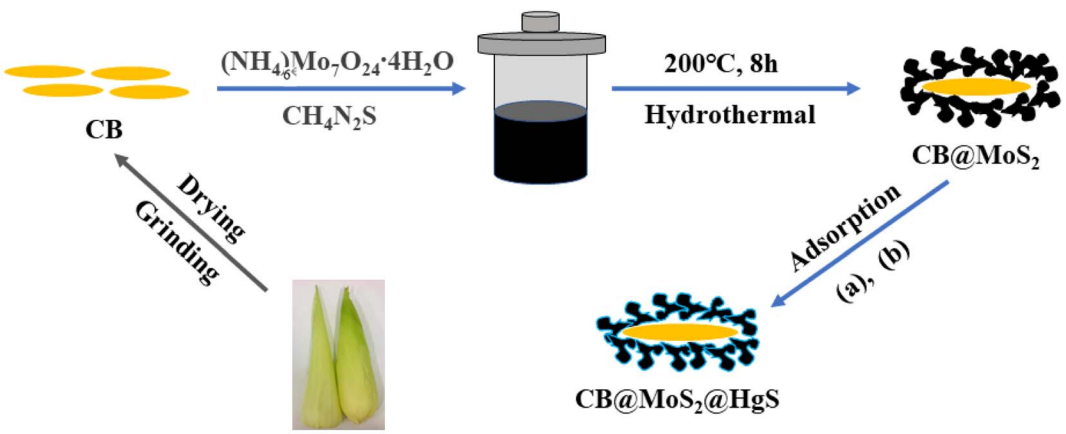

(a): $MoS_2 + Hg^{2+} \longrightarrow HgS + Mo^{4+}$

(b): $\equiv MoS_2 + Hg(II) \longrightarrow \equiv MoS_2\text{-}Hg(II)$

$(CB)\text{-}OH + Hg(II) + HO\text{-}(CB) \longrightarrow (CB)\text{-}OH\cdots Hg(II)\cdots HO\text{-}(CB)$

$(CB)\text{-}NH_2 + Hg(II) + NH_2\text{-}(CB) \longrightarrow (CB)\text{-}NH_2\cdots Hg(II)\cdots NH_2\text{-}(CB)$

Fig. 1 The preparation route and adsorption mechanism of CB@MoS_2.

$$R = \frac{(C_0 - C_t)}{C_0} \times 100\% \quad (2)$$

Among them, the adsorption capacity at equilibrium is represented by Q_t (mg g^{-1}); the initial concentration of Hg(II) ions is represented by C_0 (mg L^{-1}); the equilibrium concentration of Hg(II) ions is represented by C_t (mg L^{-1}); m (g) and V (mL) are the amount of adsorbent (g) and solution volume (mL); R represents the removal rate (%).

3. Results and discussion

3.1. Structure and morphology of the adsorbent

3.1.1. FT-IR analysis. The FT-IR spectra of the adsorbent were shown in Fig. 2(a). The characteristic peaks of the O–H and C–H groups were located at 3439 and 2929 cm^{-1}, which were their stretching vibrations. Due to the stretching vibration of the –NH_2 group, an adsorption peak appeared at 1620 cm^{-1}.[21] According to the peaks at 1032 and 1161 cm^{-1}, the stretching vibration of the C–O group was affirmed.[22] Compared with CB, the new peak at 614 cm^{-1} corresponded to the infrared stretching vibration of C–S,[23] and the decreased of peak strength at 3439, 1620, 1161 and 1032 cm^{-1} further indicated that MoS_2 was successfully introduced to the surface of CB.

3.1.2. TG analysis. The thermal decomposition behavior of the adsorbent was shown in Fig. 2(b). According to the TG curve, the CB and CB@MoS_2 maintained good thermal stability before 200 °C, which had good thermal stability and met the practical application as the adsorbent. After 250 °C, the mass loss of CB@MoS_2 began to occur because of the thermal decomposition of organic constituents in CB. The organic compound in CB completely decomposed at 600 °C, the content of MoS_2 in CB@MoS_2 was about 11% by the comparation of the residual in CB and CB@MoS_2.

3.1.3. XRD analysis. Fig. 2(c) showed the XRD patterns of the adsorbent at the 2θ range of 5–90°. It could be seen that the prominent diffraction peaks at 2θ = 33.36°, 41.67°, 44.79° and 50.91° were accurately attributed to the (100), (103), (105) and (110) reflections of MoS_2. The results indicated that the surface of CB was successfully modified with MoS_2.[24]

3.1.4. SEM analysis. Fig. 3 showed the surface morphology of the adsorbent. The surface of the CB was smooth, and the block solid was uniform, as shown in Fig. 3(a) and (b). Therefore, the roughness of the CB surface in Fig. 3(c)–(f) proved that MoS_2 with a flower-like structure had been successfully loaded on the CB solid surface. In addition, TEM images showed the sheet-like structure of CB and the flower-like nano-sheet structure of MoS_2 (see Fig. S1 in the ESI†).

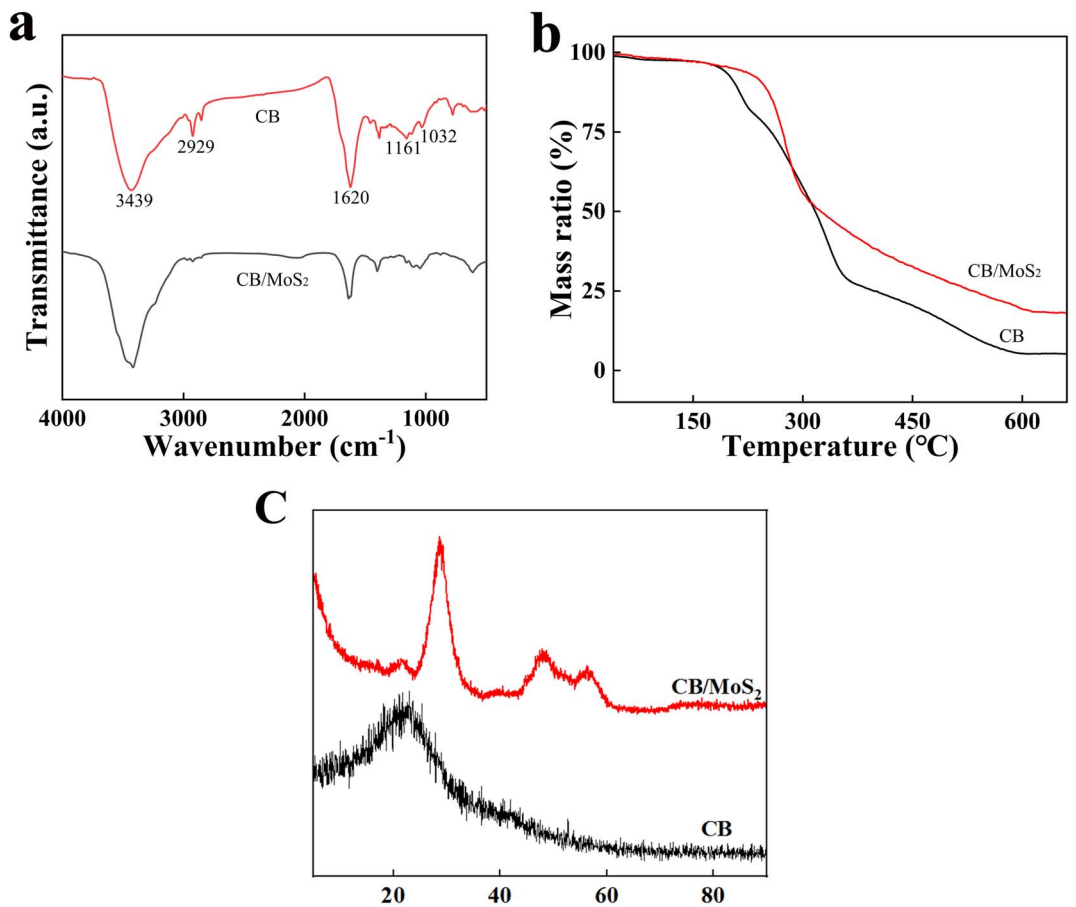

Fig. 2 (a) FT-IR spectra of CB and CB@MoS_2; (b) TGA curves of CB and CB@MoS_2; (c) XRD patterns of CB and CB@MoS_2.

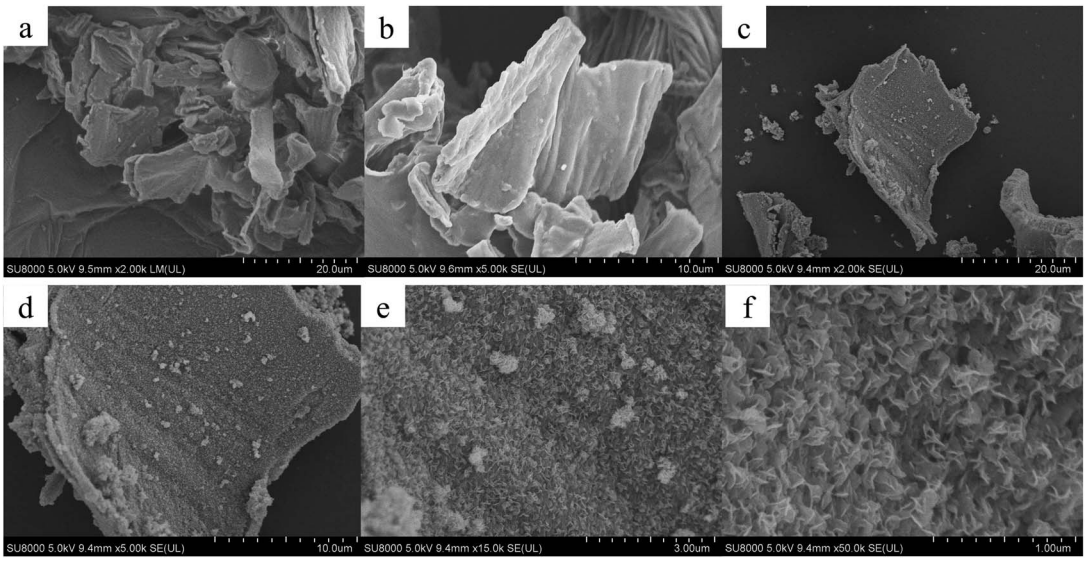

Fig. 3 SEM images of CB (a and b), CB@MoS_2 (c–f).

3.2. Effect of mass ratio of CB and MoS_2 on adsorption

Fig. 4(a) showed the effect of the different mass ratios of CB and MoS_2 on the adsorption capacity of Hg(II). It could be clearly seen that the adsorption capacity of CB@MoS_2 composite material could reach the maximum when the ratio was 6 : 1–8 : 1, and when the ratio was 9 : 1–11 : 1, its adsorption capacity showed a downward trend. Therefore, the ratio of 8 : 1 was selected as the best ratio for the next adsorption study.

3.3. Effect of adsorbent dosage

The effect of adsorbent dosage was explored by adding a certain amount of adsorbent (5–30 mg) to the Hg(II) aqueous solution. Fig. 4(b) showed the removal rate under different doses. As the amount of adsorbent increased, the removal rate increased, and when the amount of adsorbent was 15 mg, 99.75% of Hg(II) ions could be removed, and then the removal rate value remains basically unchanged with adsorbent dosage. Therefore, CB@MoS_2 with an optimal adsorbent dosage of 15 mg was selected for removing Hg(II) in water.

3.4. Effect of pH value on adsorption

The effect of the initial pH on the adsorption performance of the material is very critical, because it affects the ionization level of the material and the form of Hg(II) ions.[25] The effect of pH on the adsorption capacity of Hg(II) and Zeta potentials by CB@MoS_2 were shown in Fig. 5(a). Based on the image below, the pH value increased from 2 to 8, and the zeta potential on the surface gradually decreased. When the pH value was lower than 4.1, the active surface of CB@MoS_2 had a positive charge. First, the adsorption capacity increased significantly as the pH value went from 2.0 to 4.0. As the pH value increased from 4.0 to 8.0, the adsorption capacity was found to decrease. The

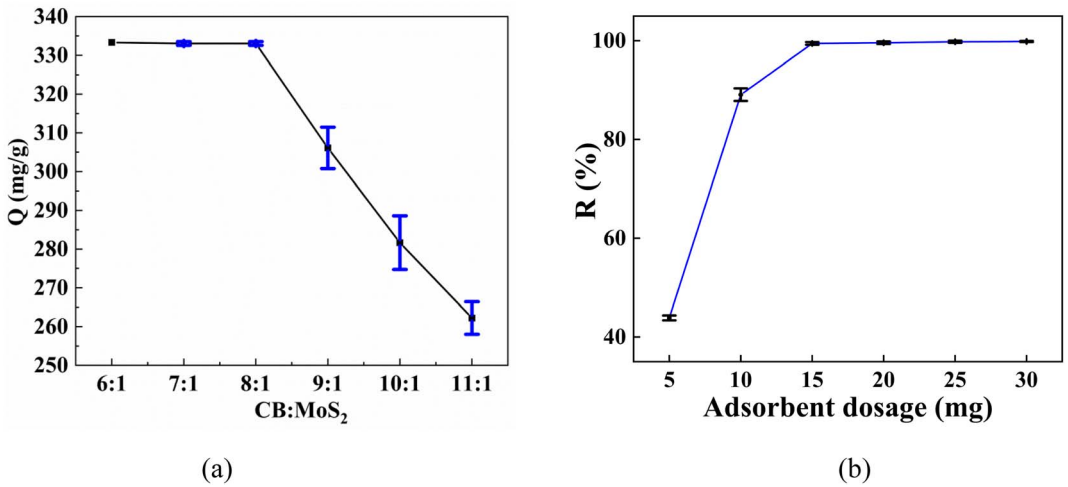

Fig. 4 (a) Effect of the mass ratios of CB and MoS_2 on the adsorption capacity of Hg(II); (b) effect of adsorbent dosage on uptake of Hg(II).

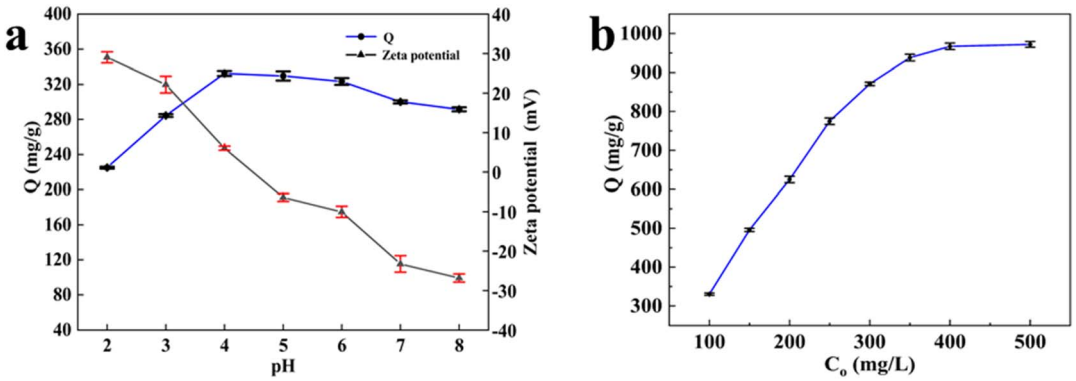

Fig. 5 (a) Effect of pH on adsorption of Hg(II) ions; (b) effect of initial concentration on adsorption of Hg(II) ions.

following the fact could be explained: At lower pH, the binding site was occupied by Hg(II) competing with the high concentration of H^+ in the solution, resulting in electrostatic repulsion, so that the formation of Hg(II) coordination complexes would be prevented. The zeta potential of CB@MoS_2 gradually decreased as the pH increased from 2 to 4, which reduced the electrostatic repulsion of functional groups and increased the adsorption capacity rapidly. When the pH value was greater than 4.1, Hg(II) cations were easily precipitated in the form of $Hg(OH)^+$ or $Hg(OH)_2$, for which adhere to the active center and hindered the next adsorption.[26] So the optimal pH of the adsorbent was 4.

3.5. Effect of Hg(II) concentration and adsorption isotherm

3.5.1. Effect of initial Hg(II) ion concentration on Hg(II) ion adsorption. To further illustrate the behavior of equilibrium adsorption, Fig. 5(b) showed the effect of different initial Hg(II) concentrations. Experimental results showed that the adsorption capacity increased significantly when the initial

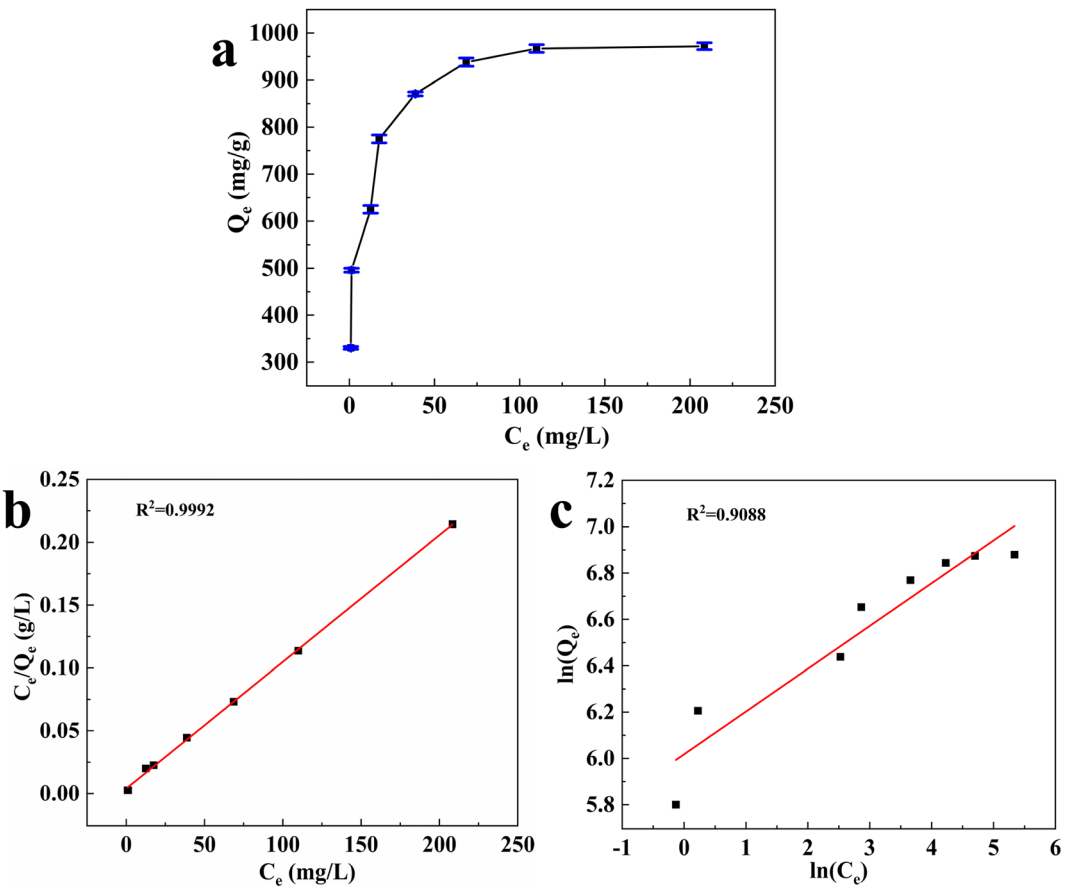

Fig. 6 (a) Experimental isotherm of Ce/Qe; (b) Langmuir isotherm plots; (c) Freundlich isotherm plots.

concentration of Hg(II) increased at the range of 100 to 350 mg L^{-1}, this was due to the increased collision probability between the active sites of the adsorbent and Hg(II). The active sites of the adsorbent tended to be saturated when the initial Hg(II) concentration was higher than 350 mg L^{-1}, and the available binding sites were competitively used by excess metal ions, so the adsorption capacity for Hg(II) tended to balance.

3.5.2. Adsorption isotherm. The Langmuir (L) isotherm model, Freundlich (F) isotherm model and Ce/Qe are applied to study the adsorption equilibrium, as shown in Fig. 6(a)–(c), and the corresponding parameters were listed in Table S1.† The R^2 value ($R^2 = 0.9992$) of L isotherm model was higher than that of F isotherm model ($R^2 = 0.9088$), which indicated that the experimental data was more compatible with the L isotherm model. The adsorption process was a single-layer adsorption, and there were typical adsorption sites on flower-shaped MoS_2.[27] In addition, according to the calculation of the L isotherm model, it could be concluded that the maximum adsorption capacity was 990.10 mg g^{-1}.

3.6. Effect of contact time on adsorption and adsorption kinetics

3.6.1. Effect of contact time. The influence of contact time on the adsorption of Hg(II) at 298 K was shown in Fig. 7(a). First, within 0–30 min, the adsorption capacity of this process increased sharply. At 30 min, its adsorption capacity and removal rate reached 279.17 mg g^{-1} and 83.75%, respectively. From 30 to 120 min, with the increase of time, the adsorption capacity tended to balance. At 120 min, the adsorption capacity could reach 332.50 mg g^{-1}, and the removal rate was 99.75%. At the first stage of 0–30 min, the adsorbent could be completely dispersed because of numerous adsorption sites on the surface of CB@MoS_2. Hg(II) ions occupied most of the effective positions at 30–120 min, then electrostatic repulsion occurred between the surface of CB@MoS_2 and Hg(II) ions in the solution. Under the same experimental conditions as above, the adsorption capacity of CB was only 37.5 mg g^{-1} and the adsorption removal rate was only 22.50%.

For comparison, the adsorption capacity of the reported biomass adsorbents was shown in Table 1. It was found that the adsorption capacity of CB@MoS_2 was higher than the reported adsorbents listed in Table 1.

3.6.2. Kinetic studies. The study of adsorption kinetics plays an important role in exploring the optimal reaction rate and adsorption mechanism. As shown in Fig. 7(b)–(d), the adsorption experimental data through the pseudo-first-level, second-level model and intraparticle diffusion model were summarized in Table S2.† According to the fitting results of the above models, the R^2 values of the pseudo second-order equation for Hg(II) were 0.991. The experimental adsorption capacity ($Q_{e,exp}$ = 332.50 mg g^{-1}) was closed to the theoretical value, which was more in line with the adsorption process. Therefore, the adsorption kinetics of Hg(II) on the adsorbent conformed to the pseudo-second-order equation, indicating that Hg(II) ions

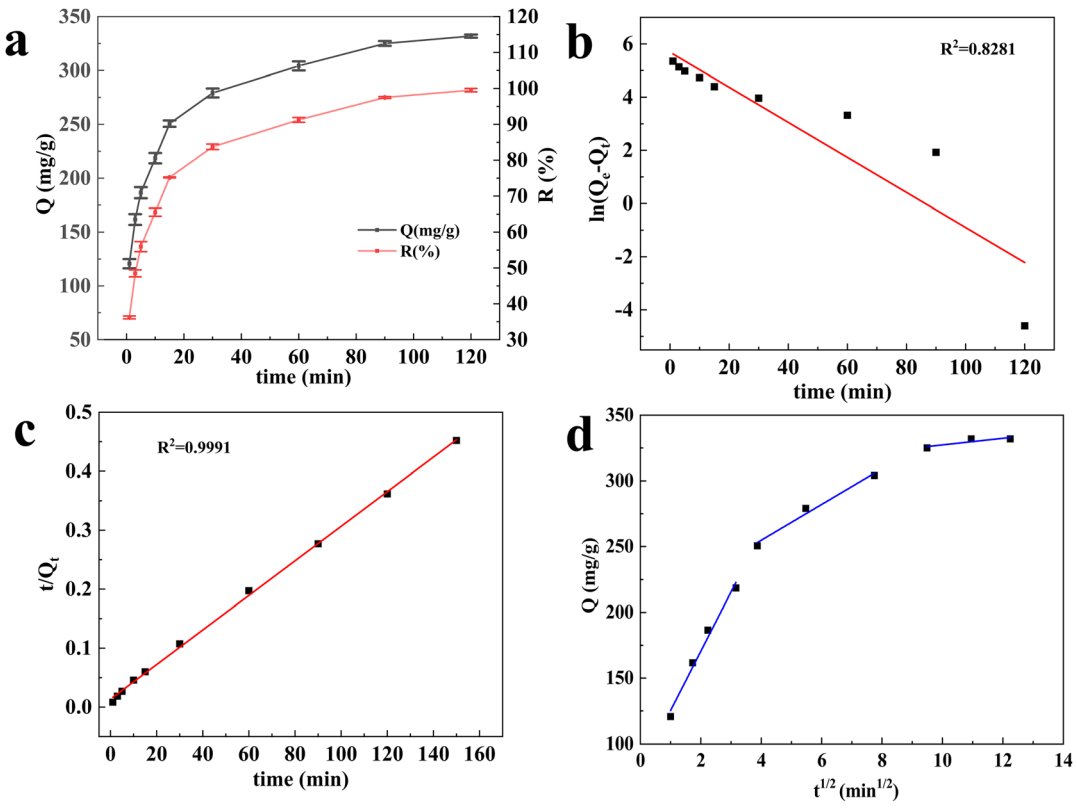

Fig. 7 (a) Effect of contact time of on adsorption Hg(II) ions onto CB@MoS_2; (b) fit of kinetic data to pseudo-second-order model; (c) fit of kinetic data to pseudo-second-order model; (d) fit of kinetic data to intraparticle diffusion model.

Table 1 Adsorption capacity of the reported biomass adsorbents

Adsorbent	Q_e (mg g^{-1})	Ref.
AT-MCS nano-biosorbent	246.00	28
Cellulose nanofibrils (CNF)	131.86	29
AC – rice husk (RH)	55.870	30
Corn cob activated carbon (CCAC)	145.80	31
PPy-Fe_3O_4/kaolin	317.10	32
PoVan/$CoFe_2O_4$@mSiO_2	263.60	33
Tannic acid cross-linking cellulose/polyethyleneimine (MCP)	247.51	34
This study (CB@MoS_2)	332.50	

adsorbed by CB@MoS_2 was mainly controlled by chemical adsorption. In addition, the fitting results of the intra-particle diffusion model and related parameters showed that the adsorption process of Hg(II) by CB@MoS_2 was divided into three stages, indicating that the adsorption rate was affected by multiple adsorption processes. First of all, a large amount of Hg(II) ions were adsorbed from the solution to the outer surface of the adsorbent at the first stage, and the slope of the fitting line K_{P1}(45.104) at this stage was the highest, which proved that the adsorption was the fastest in this process, when the outer surface was gradually saturated with adsorption, Hg(II) diffused into the second stage, in which the adsorption mainly took place on the inner surface of the adsorbent. Finally, the available adsorption siting at the third stage was almost completely occupied, and the adsorption almost reached equilibrium with the lowest fitting K_{P_3}(2.5264) at this stage.

3.7. Effect of temperature and thermodynamic analysis

Fig. 8 showed the effect of the temperature on the adsorption of Hg(II) and the corresponding thermodynamic parameters were listed in Table S3.† The adsorption capacity increased with the temperature from 298 K to 328 K, indicating that increasing the temperature was beneficial to the adsorption process.

The standard free energy change ΔG decreased with the increase of temperature, which proved that the adsorption process could proceed spontaneously. The positive enthalpy change ΔH showed that the absorption of CB@MoS_2 to Hg(II) was an endothermic reaction. The positive entropy change ΔS verified the increase in the randomness of the interface between Hg(II) and CB@MoS_2 during the adsorption process.

3.8. Effect of coexisting ions and practical application in industrial wastewater

Various coexisting cations may affect the adsorption performance in the competition. All ion concentrations are 100 mg L^{-1}. Therefore, in this work, Zn^{2+}, Ca^{2+}, Mg^{2+}, Al^{3+}, Pb^{2+}, Cu^{2+} and Ni^{2+} were used to study the effects of Hg(II) ions. As shown in Fig. 9(a), the comparison results revealed that the CB@MoS_2 exhibited good Hg(II) absorption capacity in the presence of competing cations, which proved the high selectivity to Hg(II). This is mainly because the PKsp of HgS is the largest, so that the sulfide combines with Hg first to form HgS. At the same time, the sulfur atom also had a strong complexing ability for Pb(II).[35] Therefore, when Pb(II) and Hg(II) coexist, the adsorbent would have an impact on the adsorption selectivity of Hg(II).

Based on the above experiments, the practical application of CB@MoS_2 for the adsorption of Hg(II) in industrial wastewater was investigated. The adsorbent (15 mg) was put into the industrial wastewater adjusted to the optimal pH value (pH = 4.0, c = 77.5 mg L^{-1}) for adsorption comparison, it was found that at the optimal pH value, the adsorption capacity was 216.67 mg g^{-1}, and the removal rate was 83.87%.

3.9. Regeneration experiments

The regeneration experiments are particularly important for evaluating the stability of CB@MoS_2 and reducing wastewater treatment costs. In the desorption experiment, since HgS is soluble in Na_2S and MoS_2 is insoluble in Na_2S,[36] it is treated with Na_2S solution to quickly elute the adsorbed mercury ions. The CB@MoS_2 attached with Hg(II) was added into a Na_2S solution (20 mL, 1 mol L^{-1}), then washed with water several times, dried and reused in the next cycle. As seen in Fig. 9(b), CB@MoS_2 still exhibited excellent adsorption performance

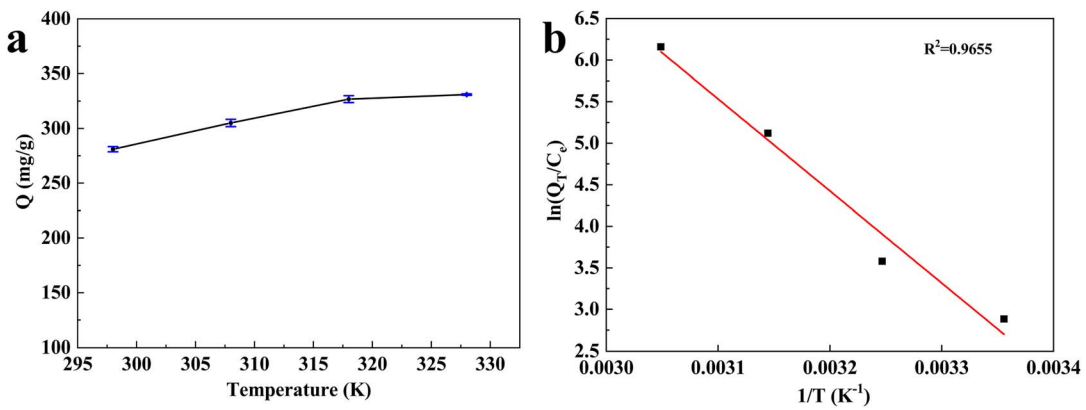

Fig. 8 (a) Effect of the temperature on the adsorption of Hg(II), (b) plot dependence of ln(Q_t/C_e) on 1/T for the estimation of thermodynamic parameters.

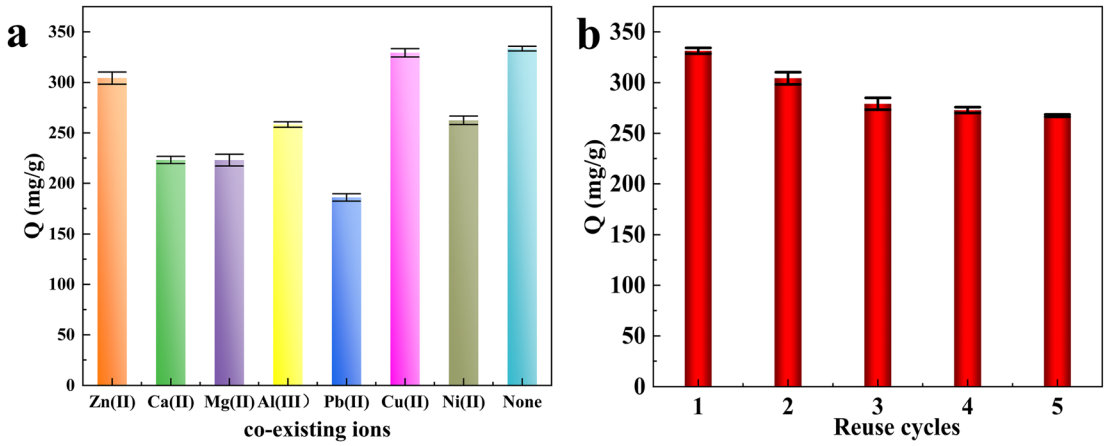

Fig. 9 (a) The effect of coexisting cations on the Hg(II) adsorption, (b) regeneration test of CB@MoS_2.

after five adsorption–desorption cycles. These results indicated that the prepared CB@MoS_2 could be effectively regenerated.

3.10. Possible adsorption mechanism of CB@MoS_2

In order to explore the adsorption mechanism of Hg(II), the chemical structure and composition of CB@MoS_2 before and after Hg(II) adsorption was analyzed using FT-IR, XRD and XPS techniques. The corresponding results were shown in Fig. S2.†

According to Fig. S2,† the XRD patterns of CB@MoS_2@Hg confirmed the presence of HgS on the MoS_2 surface, and the FT-IR spectra of CB/MoS_2@Hg showed that the peak intensity was obviously weakened, which indicating that –OH or –NH_2 groups might be involved in the adsorption of Hg(II).

XPS technology at the range of 0–800 electron volts was used to measure the binding energy of CB@MoS_2 and CB@MoS_2@-Hg surface components. As shown in Fig. 10(a), compared with CB@MoS_2, new binding energy bands could be observed in the CB@MoS_2@Hg spectrum, including Hg 4f, Hg $4d^5$ and Hg $4d^3$, which confirmed the adsorption of Hg(II) on CB@MoS_2. The appearance of Hg $4f^{5/2}$ and Hg $4f^{7/2}$ at 104.56 eV and 100.54 eV, respectively, which confirmed that CB@MoS_2 had adsorbed Hg(II) (Fig. 10(b)). The comparison before and after adsorption revealed that, except for the C–C, the binding energy of the C–O, O–H and –NH_2 had slightly changed (Fig. 10(c–e)). It showed that the –OH and –NH_2 groups were chelated with Hg(II), which was consistent with the results of FT-IR spectra analysis. Furthermore, the S 2p spectra of CB@MoS_2 were shifted from

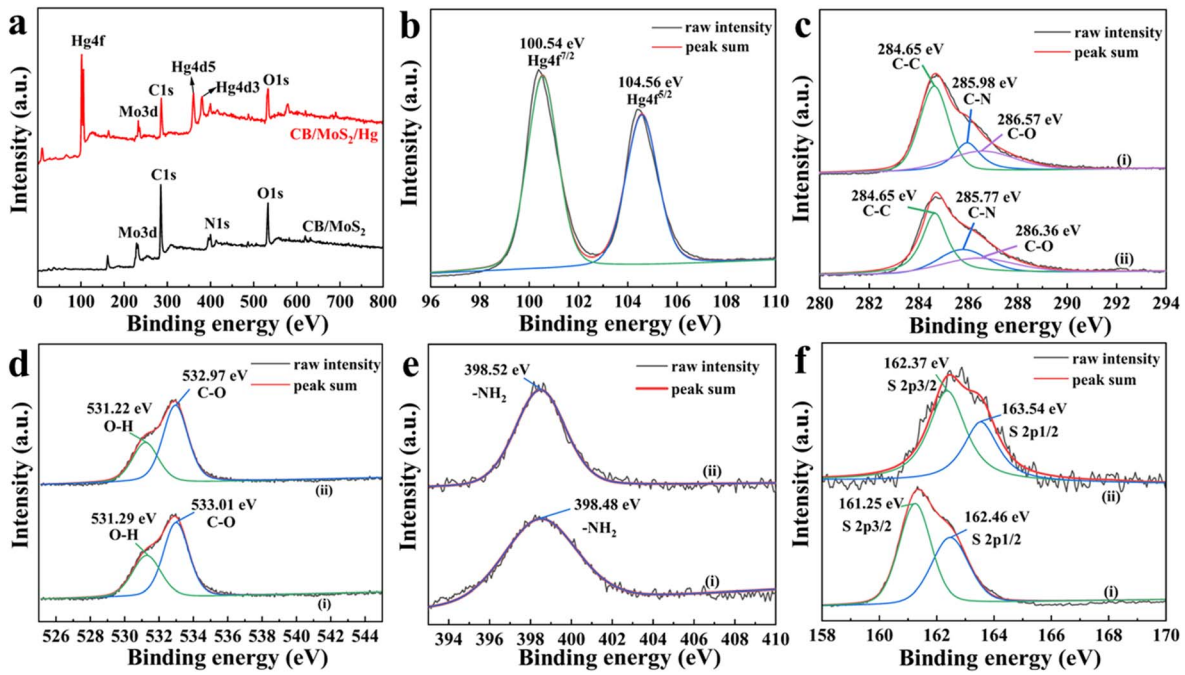

Fig. 10 (a) Full survey XPS spectra; (b) high resolution Hg 4f; (c) C 1s; (d) O 1s; (e) N 1s and (f) S 2p spectra of CB@MoS_2 (i) before and (ii) after Hg(II) adsorption.

162.46 eV of S $2p^{1/2}$ and 161.25 eV of S $2p^{3/2}$ to 163.54 eV and 162.37 eV (Fig. 10(f)). The intensity of the peak was reduced, and the results indicated that the sulfur group was also chelated with mercury.

4. Conclusions

In summary, we reported effective mercury adsorbed materials CB@MoS_2 using hydrothermal method. The structure of CB@MoS_2 was confirmed by FI-IR, XRD, SEM and TEM. The CB@MoS_2 exhibited excellent adsorption performance with the adsorption capacity of 332.50 mg g^{-1} and removal rate of 99.75% at 120 min, meanwhile, it had good selectivity and reutilization for Hg(II) ions. Moreover, the adsorption performance conformed to the pseudo-second-order model, the L isotherm model and belonged to the spontaneous endothermic process. All in all, the results showed that CB@MoS_2 was a fast and economical adsorbent, which have great prospects for removing Hg(II) in industrial wastewater.

Conflicts of interest

There are no conflicts to declare.

Acknowledgements

This work was supported by the Natural Science Foundation of Liaoning Province (2022-NLTS-15-03) and Science Research Project of Educational Department of Liaoning Province (LNSJYT202014).

References

1 K. Chen, Z. Zhang, K. Xia, X. Zhou, Y. Guo and T. Huang, *ACS Omega*, 2019, **4**, 8568–8579.
2 Z. Zhang, K. Xia, Z. Pan, C. Yang, X. Wang, G. Zhang, Y. Guo and R. Bai, *Appl. Surf. Sci.*, 2020, **500**, 143970.
3 Y. Zhao, K. Xia, Z. Zhang, Z. Zhu, Y. Guo and Z. Qu, *Nanomaterials*, 2019, **9**, 455.
4 A. M. Donia, A. A. Atia and K. Z. Elwakeel, *J. Hazard. Mater.*, 2008, **151**, 372–379.
5 M. K. Uddin, *Chem. Eng. J.*, 2017, **308**, 438–462.
6 B. Merzouk, B. Gourich, A. Sekki, K. Madani and M. Chibane, *J. Hazard. Mater.*, 2009, **164**, 215–222.
7 T. A. Kurniawan, G. Y. Chan, W. H. Lo and S. Babel, *Chem. Eng. J.*, 2006, **118**, 83–98.
8 Z. Yu, Q. Dang, C. Liu, D. Cha, H. Zhang, W. Zhu, Q. Zhang and B. Fan, *Carbohydr. Polym.*, 2017, **172**, 28–39.
9 F. Lu and D. Astruc, *Coord. Chem. Rev.*, 2018, **356**, 147–164.
10 P. M. Godwin, Y. Pan, H. Xiao and M. T. Afzal, *J. Bioresour. Bioprod.*, 2019, **4**, 31–42.
11 C. Xiong, L. Pi, X. Chen, L. Yang, C. Ma and X. Zheng, *Carbohydr. Polym.*, 2013, **98**, 1222–1228.
12 F. Ke, L. G. Qiu, Y. P. Yuan, F. M. Peng, X. A. Jiang, J. Xie, Y. H. Shen and J. F. Zhu, *J. Hazard. Mater.*, 2011, **196**, 36–43.
13 T. Luo, X. Tian, C. Yang, W. Luo, Y. Nie and Y. Wang, *J. Agric. Food Chem.*, 2017, **65**, 7153–7158.
14 Z. Wang and B. Mi, *Environ. Sci. Technol.*, 2017, **51**, 8229–8244.
15 C. L. Fausey, I. Zucker, D. E. Lee, E. Shaulsky, J. B. Zimmerman and M. Elimelech, *ACS Appl. Mater. Interfaces*, 2020, **12**, 18446–18456.
16 M. Hu, H. Tian and J. He, *ACS Appl. Mater. Interfaces*, 2019, **11**, 19200–19206.
17 I. R. Pala and S. L. Brock, *ACS Appl. Mater. Interfaces*, 2012, **4**, 2160–2167.
18 L. Huang, M. He, B. Chen and B. Hu, *J. Mater. Chem. A*, 2015, **3**, 11587–11595.
19 G. Yang, H. Han, C. Du, Z. Luo and Y. Wang, *Polymer*, 2010, **51**, 6193–6202.
20 Z. Wang, J. Zhang, T. Wen, X. Liu, Y. Wang, H. Yang, J. Sun, J. Feng, S. Dong and J. Sun, *Sci. Total Environ.*, 2020, **699**, 134341–134351.
21 L. Guo, S. X. Wang, L. Zhang, T. Hu, S. Cheng, L. K. Fu and C. Xiong, *Environ. Pollut.*, 2019, **244**, 938–946.
22 R. K. Liew, W. L. Nam, M. Y. Chong, X. Y. Phang, M. H. Su, P. N. Y. Yek, N. L. Ma, C. K. Cheng, C. T. Chang and S. S. Lam, *Process Saf. Environ.*, 2018, **115**, 57–69.
23 C. Xiong, S. Wang, L. Zhang, Y. Li, Y. Zhou and J. Peng, *J. Mol. Liq.*, 2018, **254**, 340–348.
24 J. Sun, Y. Shen and X. Hu, *Polym. Bull.*, 2018, **75**, 653–667.
25 Y. Fu, Y. Sun, Z. P. Chen, S. M. Ying, J. W. Wang and J. S. Hu, *Sci. Total Environ.*, 2019, **691**, 664–674.
26 H. Ge and T. Hua, *Carbohydr. Polym.*, 2016, **153**, 246–252.
27 D. G. Trikkaliotis, A. K. Christoforidis, A. C. Mitropoulos and G. Z. Kyzas, *Carbohydr. Polym.*, 2020, **234**, 115890–115903.
28 C. Hou, D. Zhao, S. Zhang and Y. Wang, *Colloid Polym. Sci.*, 2018, **296**, 547–555.
29 V. Bisla, G. Rattan, S. Singhal and A. Kaushik, *Int. J. Biol. Macromol.*, 2020, **161**, 194–203.
30 Z. Liu, Y. Sun, X. Xu, J. Qu and B. Qu, *ACS Omega*, 2020, **5**, 29231–29242.
31 Z. Liu, Y. Sun, X. Xu, X. Meng and B. Qu, *Bioresour. Technol.*, 2020, **306**, 123154–123160.
32 Z. Lin, Z. Pan, Y. Zhao, L. Qian, J. Shen, K. Xia, Y. Guo and Z. Qu, Removal of Hg2+ with Polypyrrole-Functionalized Fe_3O_4/Kaolin: Synthesis, Performance and Optimization with Response Surface Methodology, *Nanomaterials*, 2020, **10**(7), 1370.
33 L. Qian, Z. Zeng, S. Zhang, K. Xia and Y. Guo, Magnetic poly-o-vanillin-functionalized core–shell nanomaterials as a smart sorbent for scavenging mercury(II) from aqueous solution, *New J. Chem.*, 2021, **45**(32), 14724–14738.
34 Y. Sun, Y. Wu, Y. Fu, C. Y. Yang, J. W. Jiang, G. Yan and J. S. Hu, *Int. J. Biol. Macromol.*, 2021, **182**, 1120–1129.
35 Q. Wang, L. Peng, Y. Gong, F. Jia, S. Song and Y. Li, *J. Mol. Liq.*, 2019, **282**, 598–605.
36 Z. Qu, L. Yan, L. Li, J. Xu, M. Liu, Z. Li and N. Yan, *ACS Appl. Mater. Interfaces*, 2014, **6**, 18026–18032.